2-4-2014

Chiral Symmetry Breaking And Surface Faceting In Chromonic Liquid Crystal Droplets With Giant Elastic Anisotropy

J. Jeong

Z. S. Davidson

Peter J. Collings
Swarthmore College, pcollin1@swarthmore.edu

T. C. Lubensky

A. G. Yodh

Recommended Citation

J. Jeong, Z. S. Davidson, Peter J. Collings, T. C. Lubensky, and A. G. Yodh. (2014). "Chiral Symmetry Breaking And Surface Faceting In Chromonic Liquid Crystal Droplets With Giant Elastic Anisotropy". *Proceedings Of The National Academy Of Sciences*. Volume 111, Issue 5. 1742-1747. DOI: 10.1073/pnas.1315121111
https://works.swarthmore.edu/fac-physics/144

Chiral symmetry breaking and surface faceting in chromonic liquid crystal droplets with giant elastic anisotropy

Joonwoo Jeong[a,1], Zoey S. Davidson[a], Peter J. Collings[a,b], Tom C. Lubensky[a], and A. G. Yodh[a]

[a]Department of Physics and Astronomy, University of Pennsylvania, Philadelphia, PA 19104; and [b]Department of Physics and Astronomy, Swarthmore College, Swarthmore, PA 19081

Edited by Jonathan V. Selinger, Kent State University, Kent, OH, and accepted by the Editorial Board December 20, 2013 (received for review August 12, 2013)

Confined liquid crystals (LC) provide a unique platform for technological applications and for the study of LC properties, such as bulk elasticity, surface anchoring, and topological defects. In this work, lyotropic chromonic liquid crystals (LCLCs) are confined in spherical droplets, and their director configurations are investigated as a function of mesogen concentration using bright-field and polarized optical microscopy. Because of the unusually small twist elastic modulus of the nematic phase of LCLCs, droplets of this phase exhibit a twisted bipolar configuration with remarkably large chiral symmetry breaking. Further, the hexagonal ordering of columns and the resultant strong suppression of twist and splay but not bend deformation in the columnar phase, cause droplets of this phase to adopt a concentric director configuration around a central bend disclination line and, at sufficiently high mesogen concentration, to exhibit surface faceting. Observations of director configurations are consistent with Jones matrix calculations and are understood theoretically to be a result of the giant elastic anisotropy of LCLCs.

emulsions | complex colloids

The director configurations of confined liquid crystals exhibit a rich phenomenology, the physics of which is determined by a delicate interplay of topology, elastic free energy, and anchoring conditions at the boundaries (1–12). Droplets present arguably the simplest and most symmetric confining container for liquid crystals. Droplets of thermotropic liquid crystals (TLCs) and the manipulation of their director configurations, for example, are actively studied, in part because of their demonstrated use as core materials in display technologies (3, 13) and their potential applications ranging from biosensors (14, 15) to microlasers (16). Indeed, significant fundamental and technological progress has been made with TLC droplets, because their bulk elasticity and surface anchoring phenomena are now well understood and easily controlled.

Lyotropic chromonic liquid crystals (LCLCs) are composed of organic, charged, and plank-like mesogens that self-assemble in water into columnar aggregates via noncovalent electrostatic, excluded volume, hydrophobic, and pi–pi stacking interactions (17–20). The aggregates, in turn, assemble into nematic or columnar phases, depending on temperature and concentration. A variety of organic molecules such as dyes, drugs, and biomolecules form LCLCs (17–28). However, far less is known about the fundamental science and applications potential of LCLCs than the more-studied TLCs. Indeed, basic properties of LCLCs, including aggregate size distribution and formation dynamics, bulk elasticity, and surface anchoring are neither fully characterized nor understood and are the subject of exciting ongoing research. Only recently, for example, have measurements been made of fundamental properties, such as the Frank–Oseen elastic constants (28, 29), of any LCLC, and they have revealed unusual concentration and temperature dependences of the splay and bend moduli and a twist modulus that is unusually small compared with the other two.

Here, we explore the behavior of aqueous LCLCs droplets suspended in a background oil phase. The droplets provide an excellent platform for the study of basic LCLC properties because of their highly symmetric finite-volume confining geometry and, usually, their uniform boundary conditions. Our study investigates droplets similar to those in "classic" thermotropic LCs for which bulk elasticity and anchoring are easily characterized. Further, droplet size is more easily controlled in the water-in-oil emulsions than in systems at nematic–isotropic coexistence studied in previous work (9, 30–32). In particular, the water-in-oil emulsion system permits independent control of the continuous background phase into which one can add chemicals such as surfactants and through which one can regulate LCLC concentration to create isotropic, nematic, and columnar LCLC phases within the same drop.

Specifically, we investigate configurations of Sunset Yellow FCF (SSY) LCLCs in surfactant-stabilized spherical water droplets. The experiments reveal a variety of unusual droplet types arising from nematic LCLCs' very small twist modulus, from their room-temperature columnar phase, and from the planar anchoring of their aggregates at an oil–water interface. In the nematic phase, the director adopts a chiral-symmetry-breaking, twisted-bipolar configuration with an extraordinarily large twist revealed by polarized optical microscopy (POM). These droplets provide an archetypical example of an exotic structure that can be produced by the combination of geometric frustration and giant elastic anisotropy. In droplets of the columnar phase, which occurs at higher mesogen concentration, columns wrap in concentric circles around a central director disclination line while retaining their lattice structure. Interestingly, the lattice structure causes surface faceting of the soft boundary as the mesogen concentration is further increased.

Significance

Lyotropic chronomic liquid crystals (LCLCs) are water-based systems consisting of planar molecules that form aligned stacks in the nematic phase that develop two-dimensional crystalline order upon cooling to the columnar phase. They are characterized by an unusually small resistance to twist distortions. This work explores the interplay of giant elastic anisotropy and geometrical frustration imposed by boundary conditions in droplets, demonstrating, in particular, spontaneous formation in the nematic phase of chiral patterns from achiral building blocks and of central line defects and surface faceting in the columnar phase. Because LCLCs are water-loving, these findings about the combined effects of anisotropic elasticity, confinement, and frustration take steps toward tapping applications for liquid crystals in aqueous environments.

Author contributions: J.J., Z.S.D., P.J.C., T.C.L., and A.G.Y. designed research; J.J., Z.S.D., and T.C.L. performed research; J.J., Z.S.D., P.J.C., T.C.L., and A.G.Y. analyzed data; and J.J., Z.S.D., P.J.C., T.C.L., and A.G.Y. wrote the paper.

The authors declare no conflict of interest.

This article is a PNAS Direct Submission. J.V.S. is a guest editor invited by the Editorial Board.

[1]To whom correspondence should be addressed. E-mail: jjeong@sas.upenn.edu.

This article contains supporting information online at www.pnas.org/lookup/suppl/doi:10.1073/pnas.1315121111/-/DCSupplemental.

Results and Discussion

Nematic Phase LCLC Droplets. The usual director configuration for nematic TLCs confined to a sphere with tangential boundary conditions is the bipolar configuration (3, 4, 33), shown in Fig. 1*A*; in such droplets there are two surface defects, called Boojums, located at the North and South Poles, and the director has no azimuthal component. In Fig. 1*A*, the black dots represent the surface defects, and the short yellow rods represent liquid crystal (LC) directors. Our LCLC droplets exhibit instead a chiral twisted bipolar configuration in which the director develops an azimuthal component in passing from the bipole axis connecting the Boojums, most clearly observed in the out-of-focus images of Fig. 1*B*, to the droplet surfaces as shown in Fig. 1*C*. Considering the homogeneous and isotropic nature of the background oil phase and clearly observed Boojums, we assume the observed planar anchoring is degenerate and uniform at the LCLC–oil interface (see *SI Text* for more comments and an estimation of the polar anchoring coefficient).

To investigate this configuration more deeply, we derived sets of POM images of the droplet while rotating the sample (Fig. 1*D*). In Fig. 1*D*, two surface defects in the droplet are approximately in the same plane, parallel to the substrate, an observation that is checked by examining the symmetry of the images under rotation. The patterns observed in the POM images differ significantly from the Jones matrix-simulated POM images of the bipolar configuration (Fig. 1*E*); notice, for example, that the center of the droplet in Fig. 1*E* does darken when the bipole axis is oriented parallel to either the polarizer or analyzer. By contrast, the patterns observed in the POM images are well described by a twisted bipolar configuration. Fig. 1*F* shows the Jones matrix simulation of the optical pattern of a twisted bipolar configuration that exhibits, among other features, a disconnected bright ellipse similar to that observed in Fig. 1*D* and in thermotropic chiral nematic droplets (34).

The twist angle α_0 of the director (Fig. 2*A*) at the equatorial surface relative to the bipole axis provides a quantitative characterization of the twisted bipolar structure. Physically, it is determined by the ratios K_1/K_2 and K_1/K_3 of the splay modulus to the twist and bend moduli, respectively. According to Williams (35) and to Lavrentovich and Sergan (36), a director pattern in a spherical LC droplet with planar anchoring can break chiral symmetry when K_2 is sufficiently small compared with K_1 and K_3, i.e., when $K_3/K_1 \leq 2.32\,(1 - K_2/K_1)$; the twisted bipolar configuration has been observed in TLC droplets satisfying this condition (36–38). The nematic SSY satisfies this condition for the twisted bipolar configuration (28), and the Williams' model predicts that these nematic SSY droplets should have a twist angle α_0 greater than 80° (35).

To estimate α_0, we measured the transmitted light intensity under crossed polarizers through the centers of the twisted bipolar droplets. We assume the twist angle $\alpha(\rho)$ changes linearly with the distance ρ from the bipole axis (i.e., the radial coordinate in a cylindrical coordinate system with the z axis along the bipole axis); i.e., $\alpha(\rho) = \alpha_0\rho/\rho_0(z)$ (Fig. 2*A*). Here $\rho_0(z)$ is the maximum value of ρ in a droplet at a given z. Given the remarkable similarity in the optical patterns of the nematic LCLC droplet and a thermotropic chiral nematic droplet with low chirality (34), this assumption is reasonable. Specifically, along the diameter at $z = 0$, the twist angle changes linearly on a path from surface to surface along a chord through the origin from $+\alpha_0$ (red rod) to $-\alpha_0$ (blue rod), passing through zero at the bipole axis (Fig. 2*A*). The central region can readily be approximated as the well-known planar twisted nematic cell often used in liquid crystal displays (39). Fig. 2 *B* and *C* shows the intensity transmitted through this central region as a function of the angle of polarizer with respect to the fixed analyzer. The measured intensity reported in Fig. 2*C* is the average intensity over this central region (i.e., a cylinder through the center of the droplet with a diameter ~10% of the droplet diameter). The direction of the pass axis of the analyzer is set parallel to the bipole axis.

To determine α_0, these intensity data are fit to Eq. **1** below (for details see *SI Text*), which is approximately equal to the transmitted light intensity through a corresponding planar twist cell as a function of the angle θ of the entrance polarizer (39),

$$I \approx I_0\left(\cos^2(\theta + 2\alpha_0) + \sin^2 X \sin(2\theta + 2\alpha_0)\sin 2\alpha_0\right). \quad [1]$$

Here $X^2 = (2\alpha_0)^2 + (\Gamma/2)^2$, $\Gamma = 2\pi\,\Delta n\,d/\lambda$, where λ is the wavelength of the illuminating light (i.e., 650 nm), Δn (i.e., −0.08) (22) is the difference in index of refraction for light polarized parallel versus perpendicular to the director, and I_0 (I) represents the intensity of the illumination (transmitted) light. For our droplets, the droplet diameter d is greater than 30 μm, and the expected α_0 is on the order of 1 rad; thus, it is reasonable to assume that the droplets are in the Mauguin regime in which the polarization of the light follows the director. The solid lines in Fig. 2*C* are best fits to the data (for details see *SI Text*).

Surprisingly, the measurements suggest that the nematic LCLC droplets have a very large twist angle, i.e., $\alpha_0 > 90°$. The average of $|\alpha_0|$ over 18 different droplets was $114.8 \pm 4.4°$. Note that twist angles greater than 90° were not reported experimentally in refs. 3 and 36–38, nor predicted by the largely accepted Williams' model (35). Additionally, the sign of the fitted α_0 implies a certain handedness of chirality, and both signs were observed in the

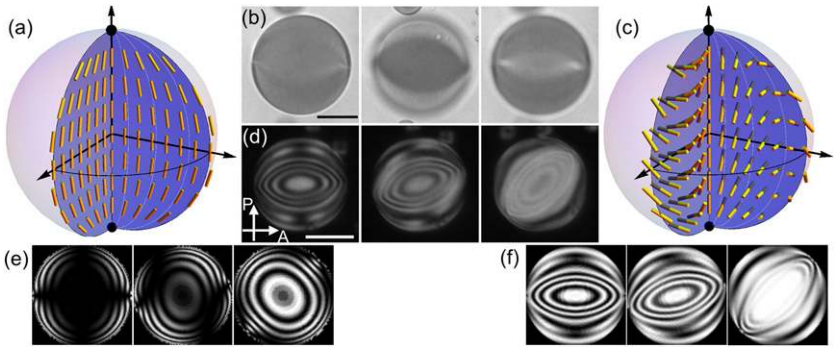

Fig. 1. Optical microscopy images of a nematic LCLC droplet and Jones matrix calculations of the patterns in droplets between crossed polarizers. Scale bar, 20 μm. Schematic diagrams of (*A*) the bipolar configuration and (*C*) the twisted bipolar configuration. Black dots represent the defects at the droplet surface and short yellow rods represent LC directors. (*B*) Bright-field microscopy images of the nematic droplet in different focal planes. (*D*) POM images of a droplet between a crossed polarizer (P) and analyzer (A); the pass-axis directions are shown as white arrows. Each column shows a droplet at a different rotation angle. Corresponding POM patterns simulated by Jones matrix calculations of light propagating through the droplet of (*E*) a bipolar configuration and (*F*) a twisted bipolar configuration.

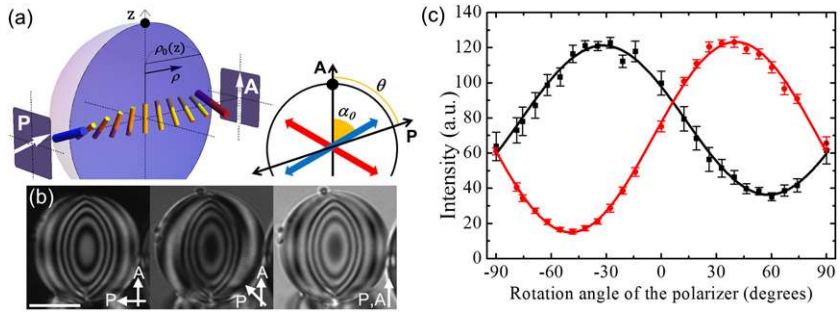

Fig. 2. Intensity of transmitted light through the centers of droplets. (*A*) Schematic diagram of the twisted bipolar configuration between polarizer (P) and analyzer (A). Black dots represent the Boojums at the droplet surface, and the line connecting them is the bipole axis. The direction of the analyzer (A) is parallel to the bipole axis connecting two defects. θ is defined by the angle between the polarizer (P) and the analyzer (A). Short yellow rods show LC directors along a chord through the center of the droplet only. Thick blue and red rods represent the entrance and exit LC directors, respectively. ρ is the radial coordinate in a cylindrical coordinate system with the z axis along the bipole axis, and $\rho_0(z)$ is the maximum value of ρ in a droplet at a given z. (*Inset*) Projection view through polarizer and analyzer; α_0 is defined as the angle between meridional lines and the entrance LC director at the surface of the droplet. (*B*) POM images of the droplet located between the polarizer (P) and analyzer (A) with directions shown as white arrows. Scale bar, 20 μm. (*C*) Intensity of the transmitted light through the center of the droplet as a function of the angle between the polarizer and the analyzer. Black and red symbols are data from two representative droplets, and the solid curves are best fits to the data using Eq. **1**. The error bars are the SDs of intensities over the central region of which the diameter is 10% of the droplet diameter.

droplet sample. Based on the number ratio between positive and negative twist angles (i.e., 7:11) across all droplets, it appears that there is no preferred handedness of chirality in these systems (i.e., within our statistical error). Interestingly, these droplets look remarkably similar to thermotropic chiral nematic droplets with a half pitch less than a diameter of the droplet, i.e., droplets in which α_0 is greater than 90° (34). We searched for correlations between α_0 and the size of the droplet for droplets with diameters in the range of 30 to 80 μm, but we found none.

Lastly, to understand this large chiral symmetry breaking in droplets at a fundamental level, we carried out a numerical calculation of elastic free energy based on a simplified director field model. To this end, we followed Xu and Crooker (34) and Xu et al. (37) and assumed a simplified director field for the twisted bipolar configuration $\boldsymbol{n}_{\rm tb} = \boldsymbol{n}_{\rm b}\cos(\alpha) + \boldsymbol{n}_{\rm c}\sin(\alpha)$, which combines the bipolar configuration $\boldsymbol{n}_{\rm b}$ and the concentric configuration $\boldsymbol{n}_{\rm c}$ (for details see *SI Text*). For the droplet calculations, we use the director field models for the bipolar configuration and the concentric configuration used by Ding and Yang (40).

Assuming a linearly changing $\alpha(\rho) = \alpha_0\rho/\rho_0(z)$, we numerically calculate the elastic free energy of each deformation mode and their sum as a function of α_0 (for details see *SI Text*) as shown in Fig. 3*A*. Note that the splay energy exhibits a minimum at $\alpha_{min} \sim$ 130°, which sets an upper bound on α_0, whereas the elastic free energy of the twist and bend deformations increases monotonically with α_0. Therefore, the total elastic free energy has its minimum at nonzero α_0. For example, for $K_2/K_1 \sim 0.09$ and $K_3/K_1 \sim 0.91$ in a 31.5% (wt/wt) SSY solution (28), the twist angle is expected to be $\alpha_0 \sim 90°$. At higher concentrations, because K_1 and K_1/K_2 and K_1/K_3 increase (28), the α_0 of the minimum elastic free energy increases and can surpass 90°. This effect is shown in Fig. 3*B* for $K_2/K_1 \sim 0.07$ and $K_3/K_1 \sim 0.67$, wherein the droplet has $\alpha_0 \sim 100°$. In practice, the evaporation of water from the droplet into the background oil phase increases the SSY concentration in the droplet from its initial value of 31.0% (wt/wt), thereby increasing K_1. It is thus reasonable for α_0 to reach values greater than 90°. Note, however, the untwisted bipolar configuration ($\alpha_0 = 0$) is preferred at sufficiently large values of K_2/K_1 as shown in Fig. 3*B*, which is consistent with the Williams condition for the twisted bipolar configuration.

To conclude this section we explore the spatial dependence of the elastic free energy in the region around the defect. Indeed, it is the behavior in the vicinity of the defect that dominates the determination of the twist angle α_0. Fig. 3*C* plots the total elastic free energy of each z/R integration range where the z axis is along the bipole axis and R is the radius of the droplet. With this notation, when $z/R = 0.8$–1, the integration volume is a spherical cap near the defect, and when $z/R = 0.0$–0.2, the integration volume is a thin disk near the droplet equator. We see that most of the elastic free energy is concentrated in the region around the defect where splay is largest. Fig. 3 *D* and *E* summarizes the contributions of splay, twist, and, bend to the energy densities of the bipolar ($\alpha_0 = 0$) and twisted bipolar ($\alpha_0 = 90$), respectively. In both cases, splay in the vicinity of the Boojum dominates the energy. This energy, however, decreases with increasing twist angle, whereas the twist and bend energy increase slowly. The equilibrium value of α_0 is determined by the balance between these two effects.

Columnar Phase LCLC Droplets. To study LCLC droplets in the columnar phase (41), the concentration of SSY in the droplet was increased by evaporation of water through the oil phase, and, as a result, the liquid crystal in the droplets experienced a phase transition from nematic to columnar phase through the coexistence region (see *SI Text* for details). Fig. 4*A* shows the columnar phase droplets that exhibit a concentric director configuration. The director field model of the concentric configuration is shown in Fig. 4*B*; here the short yellow rods and the thick black line represent the LC directors and the line defect, respectively, and the dotted white lines indicate the 2D triangular lattice of the columnar phase in the droplet. The director encircles a bend disclination line defect. Fig. 4*C* shows a sequence of POM images of the droplet at different rotation angles, along with corresponding Jones matrix calculations (Fig. 4*D*) of the concentric configuration (40). Note that both the POM images and Jones matrix calculation in the concentric configuration are quite different from those of the twisted bipolar configuration (Fig. 1 *D* and *F*). Although both patterns appear as nested ellipses, the ellipses of the concentric configuration are sharper near the ends of the major axis, e.g., compared with those of the twisted bipolar configuration. In addition, a droplet in the concentric configuration has low transmittance through crossed polarizers when the line defect is parallel to either the polarizer or the analyzer.

The concentric configuration is a result of the large elastic anisotropy of the columnar phase. The lattice structure of the 2D hexagonal columnar phase strongly suppresses twist and splay but not bend deformation. Therefore, it is natural for the columnar droplet with planar anchoring to take on the concentric configuration in which only bend deformation exists. Further, as shown in Fig. 4*B*, this configuration can maintain 2D hexagonal ordering

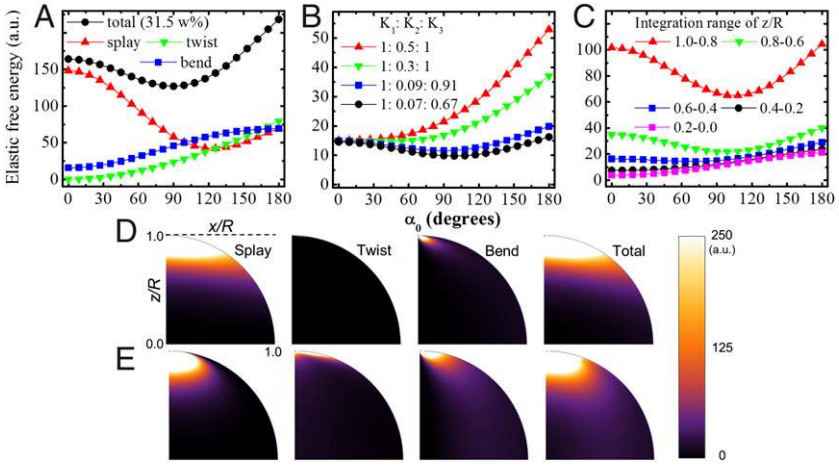

Fig. 3. Numerically calculated elastic free energy of the twisted bipolar configuration as a function of twist angle, α_0. (*A*) Splay, twist, bend elastic free energies, and their sum, for the twisted bipolar configuration droplet of 31.5% (wt/wt) SSY solution with K_1:K_2:K_3 equal to 11:1:10. (*B*) Same calculation of total elastic free energy of a twisted bipolar configuration droplet but with different K_1:K_2:K_3. (*C*) Total elastic free energy of different integration ranges of *z*/*R* in a droplet. (*D*) Elastic free-energy density of each deformation mode and their sum in the first quadrant of the droplet's cross-section for K_1:K_2:K_3 equal to 11:1:10 for the bipolar configuration (α_0= 0°) and (*E*) for the twisted bipolar configuration (α_0= 90°). Note that splay deformation in the region around the defect dominates the free-energy density but decreases substantially with twist angle α_0.

throughout the droplet except at the core line defect. Such a configuration, which is curved on a large scale even though the lattice of the columnar mesogens is not deformed, is called a developable domain (42, 43). Thus, the observed concentric configuration corresponds to a spherical developable domain, and the central disclination line defect is its 1D singularity. In contrast with the behavior in the nematic phase, the line defect cannot have an escaped structure, because splay deformation is not allowed. In addition, it is noteworthy that the line defects are large enough to be resolved in optical microscopy, e.g., width ~1 μm; in many lyotropic materials, the domain cores are too small to be resolved optically (43). The large size of the core might be closely related to unexplored properties of the LCLC columnar phase. For instance, because columnar aggregates of LCLC molecules self-assemble dynamically via noncovalent interactions and thus are semiflexible with a finite persistence length and a polydisperse length distribution (28), they might adopt a different structure when confined strongly in and around a defect core.

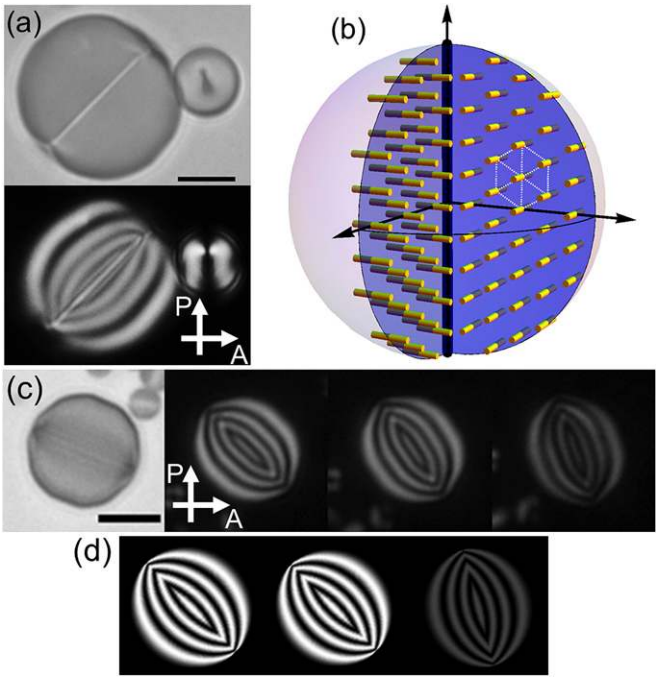

Fig. 4. Optical microscopy images of a columnar LCLC droplet and Jones matrix calculations of light patterns after passing through a droplet located between crossed polarizers. Scale bar, 10 μm. (*A*) Bright-field microscopy image (*Upper*) and POM image (*Lower*) for columnar phase droplets between a crossed polarizer (P) and analyzer (A) with pass-axis directions shown as white arrows. (*B*) Schematic diagram of the concentric configuration; the short yellow rods and the thick black line indicate the LC directors and the line defect, respectively. The hexagon of dotted white lines depicts the 2D hexagonal ordering of columns in the columnar phase. (*C*) Bright-field microscopy image and a sequence of POM images as a function of droplet orientation. (*D*) Results of Jones matrix calculations of droplet patterns for a concentric configuration.

At the very highest concentrations studied, columnar phase droplets exhibit an even more remarkable behavior: their soft surface develops facets that can be described by the Wulff construction (44, 45). As shown in Fig. 5 *A* and *B*, the columnar droplets develop facets as the LCLC concentration increases. The faceted droplets maintain notable rotational symmetry about their core line defect, indicating that the columnar order of weakly bonded aggregates is coherent over quite long distances, e.g., along a circumference of several tens of μm, as can be seen in the droplet at the upper right corner of Fig. 5*A*. For smaller droplets, the cross-section containing the line defect more closely resembles a hexagon as shown in Fig. 5*A*. This hexagonal shape can be understood using the Wulff construction to describe the equilibrium shape of a crystal in terms of its anisotropic interfacial energy. In the 2D-Wulff construction, we start with a polar plot of the interfacial energy as a function of orientation and then draw tangential lines to the polar plot. The inner envelope of these tangential lines describes the equilibrium shape of a crystal that minimizes total interfacial energy (44, 45). Specifically, in the cross-section containing the line defect shown in Fig. 5*B*, the columnar phase is a 2D crystal with hexagonal ordering. If the anisotropic interfacial energy has the sixfold symmetry shown in the polar plot of the interfacial tension (red curve in Fig. 5*C*), the Wulff construction predicts hexagonal faceting pattern (the inner envelope of gray lines in Fig. 5*C*). Rotation about either an axis connecting opposite vertices (VV′ in Fig. 5*C*) or opposite edges (EE′ in Fig. 5*C*) of the hexagon produces configurations having a hexagonal shape for each cross-section containing the rotation

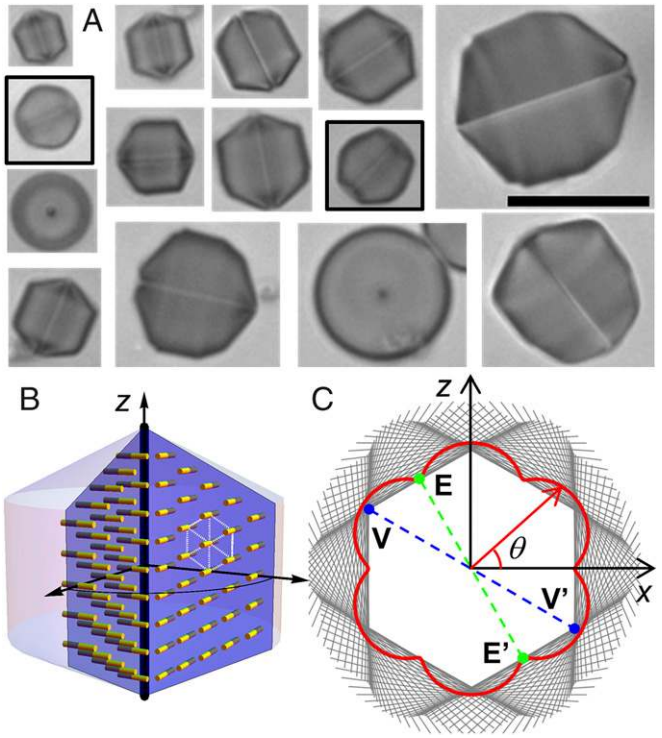

Fig. 5. Bright-field microscopy images of columnar LCLC droplets with facets and schematic diagrams of the Wulff construction of faceted droplets. (*A*) Bright-field microscopy images. Scale bar, 30 μm. The circular image with a black dot at its center is obtained when the droplet is viewed along the line defect. (*B*) Schematic diagram of the concentric configuration with facets; the short yellow rods and the thick black line indicate the LC directors and the line defect, respectively. The hexagon of dotted white lines depicts the 2D hexagonal ordering of columns in the columnar phase. (*C*) Wulff construction of hexagonal crystal. A polar plot (red curve) represents a sixfold interfacial tension of the columnar phase in the plane of 2D hexagonal ordering (*xz* plane). The Wulff construction of the polar plot predicts hexagonal crystal shown as the inner envelope of tangential lines (gray straight lines) to the polar plot. V (E) and V′ (E′) represent opposite vertices (centers of opposite edges) and dashed lines connecting them are the rotation axes of the faceted droplets.

axis. Note that a configuration having the EE′ rotation axis (E type) has more surface area than a configuration having the VV′ rotation axis (V type) at fixed volume (see *SI Text* for details and schematic diagrams). Then, it makes sense that E-type droplets with larger surface area (the droplets with a black outline in Fig. 5*A*) are observed less frequently than V-type ones. Presumably, the irregular facets in larger droplets may result from polycrystalline domains or nonuniform evaporation of water from the droplet.

Conclusion

We have made LCLC droplets with planar anchoring and studied their director configurations as a function of LCLC concentration. In nematic droplets, a very small twist elastic modulus produces an unprecedentedly large chiral symmetry breaking that can be understood theoretically using simple elastic free-energy models with large elastic anisotropy. Interestingly, despite their lack of chirality, the nematic LCLC droplets have a chiral twisted bipolar configuration similar to those observed in droplets of liquid crystals with intrinsic chirality. Columnar LCLC droplets, by contrast, exhibit a concentric director configuration with a central disclination defect, corresponding to a spherical developable domain with a 1D singularity. Additionally, because of 2D crystalline ordering of the columnar phase, the columnar droplets at the highest concentrations develop facets resulting in a hexagonal shape. We should be able to use the advantages of this emulsion system to study configurations with different boundary conditions and in various classes of external field. As in the present investigation, we expect the resultant configurations to shed light on our understanding of the delicate interplay between bulk elasticity and surface anchoring phenomena in LCLCs. Furthermore, the unique shapes and configurations formed, and the broken chiral symmetry, may offer possibilities for control and application materials based on complex colloids.

Materials and Methods

Preparation of LCLC-in-Oil Emulsion. SSY was purchased from Sigma-Aldrich at a purity of 90% (wt/wt); it was then further purified using a published precipitation method (22, 26, 46). The resultant SSY was dissolved in deionized water (18.2 MΩ cm) to make a solution of a known concentration and phase. Hexadecane [a purity of 99% (vol/vol), Sigma-Aldrich] and sorbitan monooleate (Span 80, Fluka) were used as received. Span 80 was dissolved in hexadecane and used as a nonionic surfactant for the LCLC-in-oil emulsion. See *SI Text* for the chemical structures of SSY and Span 80.

Briefly, the aqueous nematic SSY solution [31.0% (wt/wt)] was dispersed in hexadecane with a nonionic surfactant [Span 80, 2.0% (wt/wt)] by pipetting and shaking. The volume fraction of SSY solution in hexadecane was ∼1%, and the resulting nematic droplets had surface-tension stabilized spherical shapes with diameters ranging from 1 to 100 μm. A rectangular capillary with open ends (0.2 mm in height and 2 mm in width, VitroCom) was filled with this emulsion solution. While in the capillary, water in the droplet undergoes a slow evaporation through the oil phase leading to an increase of SSY concentration in the droplet and an eventual phase transition from the nematic to the columnar phase.

Observation of Droplets. Bright-field and POM images of all droplets were obtained with an inverted microscope (DM IRB, Leica Microsystems) using a 63× dry objective with coverslip-thickness correction and N.A. = 0.7. Images were taken with a black–white CCD (UP-680CL, UNIQ Vision Inc.) and quasimonochromatic illumination (center wavelength = 650 ± 2 nm, FWHM = 10 ± 2 nm) derived from a halogen lamp using a bandpass filter (P10-650, Orion). Separate absorption measurements indicate that the transmittance of the droplets at 650 nm was greater than 95%; no fluorescence was observed for 650-nm excitation. The samples were rotated on a circular stage located between a fixed polarizer and analyzer. Additionally, in this configuration images were obtained with a rotating polarizer, when both the sample and the analyzer were held fixed. Typically, once a droplet was chosen for study, all rotation experiments were conducted within 2 min so that the effects of translational and rotational diffusion of the droplet were minimal. All observations were carried out at an ambient temperature of 24 °C.

Jones Matrix Calculation. To characterize the director configurations in the droplets, the POM images of the droplet under monochromatic illumination were compared with simulations of polarized light transport through a droplet and polarizers, using the Jones calculus with 2 × 2 matrices. Specifically, the volume of a "simulated" LCLC droplet was divided into volume elements (voxels) on a 3D grid, and the LC director in each voxel was computed from a 3D director field model (3, 37, 40). Using the LCLC's estimated ordinary and extraordinary indices of refraction at the wavelength of the illumination light, the Jones matrix for each voxel was calculated (see *SI Text* for details of the Jones matrix calculation). Then, simulated plane waves were projected through the polarizer, through the simulated droplet, and through the analyzer, and the corresponding Jones matrices of the optical components and the voxels along the beam path were multiplied sequentially to derive an exit Jones vector at each pixel. The squared norms of the exit Jones vectors represent the transmitted intensities at each pixel and comprise a 2D intensity profile of the transmitted light. This profile was then compared with observation. Note that for this calculation, the effects of refraction, reflection, and diffraction by the droplet were assumed to be negligible; it is known that this approximate calculation produces reasonable simulations for large droplets with modest birefringence (3).

ACKNOWLEDGMENTS. The authors thank Matthew Lohr for helpful discussions and gratefully acknowledge financial support from the National Science Foundation (NSF) through DMR-1205463 and DMR-1120901.

1. Erdmann JH, Žumer S, Doane JW (1990) Configuration transition in a nematic liquid crystal confined to a small spherical cavity. *Phys Rev Lett* 64(16):1907–1910.
2. Poulin P, Stark H, Lubensky TC, Weitz DA (1997) Novel colloidal interactions in anisotropic fluids. *Science* 275(5307):1770–1773.
3. Drzaic P (1995) *Liquid Crystal Dispersions* (World Scientific, Singapore).
4. Lavrentovich OD (1998) Topological defects in dispersed words and worlds around liquid crystals, or liquid crystal drops. *Liq Cryst* 24(1):117–126.
5. Fernández-Nieves A, et al. (2007) Novel defect structures in nematic liquid crystal shells. *Phys Rev Lett* 99(15):157801.
6. Gupta JK, Sivakumar S, Caruso F, Abbott NL (2009) Size-dependent ordering of liquid crystals observed in polymeric capsules with micrometer and smaller diameters. *Angew Chem Int Ed Engl* 48(9):1652–1655.
7. Lopez-Leon T, Fernandez-Nieves A (2011) Drops and shells of liquid crystal. *Colloid Polym Sci* 289(4):345–359.
8. Lopez-Leon T, Koning V, Devaiah KBS, Vitelli V, Fernandez-Nieves A (2011) Frustrated nematic order in spherical geometries. *Nat Phys* 7(5):391–394.
9. Tortora L, Lavrentovich OD (2011) Chiral symmetry breaking by spatial confinement in tactoidal droplets of lyotropic chromonic liquid crystals. *Proc Natl Acad Sci USA* 108(13):5163–5168.
10. Jeong J, Kim MW (2012) Confinement-induced transition of topological defects in smectic liquid crystals: From a point to a line and pearls. *Phys Rev Lett* 108(20):207802.
11. Pairam E, et al. (2013) Stable nematic droplets with handles. *Proc Natl Acad Sci USA* 110(23):9295–9300.
12. Senyuk B, et al. (2013) Topological colloids. *Nature* 493(7431):200–205.
13. Doane JW, Vaz Na, Wu B-G, Žumer S (1986) Field controlled light scattering from nematic microdroplets. *Appl Phys Lett* 48(4):269–271.
14. Sivakumar S, Wark KL, Gupta JK, Abbott NL, Caruso F (2009) Liquid crystal emulsions as the basis of biological sensors for the optical detection of bacteria and viruses. *Adv Funct Mater* 19(14):2260–2265.
15. Lin I-H, et al. (2011) Endotoxin-induced structural transformations in liquid crystalline droplets. *Science* 332(6035):1297–1300.
16. Humar M, Musevic I (2010) 3D microlasers from self-assembled cholesteric liquid-crystal microdroplets. *Opt Express* 18(26):26995–27003.
17. Tam-Chang S-W, Huang L (2008) Chromonic liquid crystals: Properties and applications as functional materials. *Chem Commun (Camb)* (17):1957–1967.
18. Collings PJ, Dickinson AJ, Smith EC (2010) Molecular aggregation and chromonic liquid crystals. *Liq Cryst* 37(6-7):701–710.
19. Lydon J (2011) Chromonic liquid crystalline phases. *Liq Cryst* 38(11-12):1663–1681.
20. Park H, Lavrentovich OD (2012) Lyotropic chromonic liquid crystals: Emerging applications. *Liquid Crystals Beyond Displays: Chemistry, Physics, and Applications*, ed Li Q (Wiley, Hoboken, NJ), p 449.
21. Mariani P, Saturni L (1996) Measurement of intercolumnar forces between parallel guanosine four-stranded helices. *Biophys J* 70(6):2867–2874.
22. Horowitz VR, Janowitz LA, Modic AL, Heiney PA, Collings PJ (2005) Aggregation behavior and chromonic liquid crystal properties of an anionic monoazo dye. *Phys Rev E Stat Nonlin Soft Matter Phys* 72(4 Pt 1):041710.
23. Nastishin YA, et al. (2005) Optical characterization of the nematic lyotropic chromonic liquid crystals: Light absorption, birefringence, and scalar order parameter. *Phys Rev E Stat Nonlin Soft Matter Phys* 72(4 Pt 1):041711.
24. Kostko AF, et al. (2005) Salt effects on the phase behavior, structure, and rheology of chromonic liquid crystals. *J Phys Chem B* 109(41):19126–19133.
25. Nakata M, et al. (2007) End-to-end stacking and liquid crystal condensation of 6 to 20 base pair DNA duplexes. *Science* 318(5854):1276–1279.
26. Edwards DJ, et al. (2008) Chromonic liquid crystal formation by Edicol Sunset Yellow. *J Phys Chem B* 112(46):14628–14636.
27. Park H-S, Kang S-W, Tortora L, Kumar S, Lavrentovich OD (2011) Condensation of self-assembled lyotropic chromonic liquid crystal sunset yellow in aqueous solutions crowded with polyethylene glycol and doped with salt. *Langmuir* 27(7):4164–4175.
28. Zhou S, et al. (2012) Elasticity of lyotropic chromonic liquid crystals probed by director reorientation in a magnetic field. *Phys Rev Lett* 109(3):037801.
29. Nastishin YA, Neupane K, Baldwin AR, Lavrentovich OD, Sprunt S (2008) Elasticity and viscosity of a lyotropic chromonic nematic studied with dynamic light scattering. arXiv:08072669.
30. Simon KA, Sejwal P, Gerecht RB, Luk Y-Y (2007) Water-in-water emulsions stabilized by non-amphiphilic interactions: Polymer-dispersed lyotropic liquid crystals. *Langmuir* 23(3):1453–1458.
31. Simon KA, et al. (2010) Noncovalent polymerization and assembly in water promoted by thermodynamic incompatibility. *J Phys Chem B* 114(32):10357–10367.
32. Tortora L, et al. (2010) Self-assembly, condensation, and order in aqueous lyotropic chromonic liquid crystals crowded with additives. *Soft Matter* 6(17):4157–4167.
33. Volovik G, Lavrentovich O (1983) Topological dynamics of defects: Boojums in nematic drops. *Zh Eksp Teor Fiz* 58(6):1159–1166.
34. Xu F, Crooker P (1997) Chiral nematic droplets with parallel surface anchoring. *Phys Rev E Stat Nonlin Soft Matter Phys* 56(6):6853–6860.
35. Williams RD (1986) Two transitions in tangentially anchored nematic droplets. *J Phys Math Gen* 19(16):3211–3222.
36. Lavrentovich OD, Sergan VV (1990) Parity-breaking phase transition in tangentially anchored nematic drops. *Il Nuovo Cimento D* 12(9):1219–1222.
37. Xu F, Kitzerow H-S, Crooker PP (1994) Director configurations of nematic-liquid-crystal droplets: Negative dielectric anisotropy and parallel surface anchoring. *Phys Rev E Stat Phys Plasmas Fluids Relat Interdiscip Topics* 49(4):3061–3068.
38. Drzaic PS (1999) A case of mistaken identity: Spontaneous formation of twisted bipolar droplets from achiral nematic materials. *Liq Cryst* 26(5):623–627.
39. Yeh P, Gu C (2009) *Optics of Liquid Crystal Displays* (Wiley, Hoboken, NJ).
40. Ding J, Yang Y (1992) Birefringence patterns of nematic droplets. *Jpn J Appl Phys* 31(Part 1, No. 9A):2837–2845.
41. Verhoeff AA, Lekkerkerker HNW (2012) Direct observation of columnar liquid crystal droplets. *Soft Matter* 8(18):4865–4868.
42. Kleman M (1980) Developable domains in hexagonal liquid crystals. *J Phys* 41(7): 737–745.
43. Oswald P, Pieranski P (2006) *Smectic And Columnar Liquid Crystals: Concepts and Physical Properties Illustrated by Experiments* (Taylor & Francis/CRC, Boca Raton, FL).
44. Chandrasekhar S (1966) Surface tension of liquid crystals. *Mol Cryst* 2(1-2):71–80.
45. Rottman C, Wortis M (1984) Statistical mechanics of equilibrium crystal shapes: Interfacial phase diagrams and phase transitions. *Phys Rep* 103(1-4):59–79.
46. Park H-S, et al. (2008) Self-assembly of lyotropic chromonic liquid crystal Sunset Yellow and effects of ionic additives. *J Phys Chem B* 112(51):16307–16319.